The Planetary Science Journal, 7:90 (10pp), 2026 April https://doi.org/10.3847/PSJ/ae5931

Spectral Similarity in the Thermal Infrared between Sulfide-rich Carbonaceous Chondrite Meteorites, Jupiter Trojans, and Other D- and P-type Asteroids

Helena C. Bates[1], Ashley J. King[1], Kerri L. Donaldson Hanna[2], Audrey C. Martin[2,3], Joshua P. Emery[4], Neil E. Bowles[5], and Sara S. Russell[1]
[1] Natural History Museum, Cromwell Road, London, SW7 5BD, UK; h.bates@nhm.ac.uk
[2] University of Central Florida, Orlando, FL 32816, USA
[3] California Institute of Technology, Pasadena, CA 91125, USA
[4] Northern Arizona University, Flagstaff, AZ 86011, USA
[5] Oxford University, Oxford, OX1 3PU, UK
Received 2025 October 22; revised 2026 March 20; accepted 2026 March 24; published 2026 April 23

Abstract

Carbonaceous chondrite meteorites, which include the sulfide-rich "Yamato-type" chondrites (CYs), have undergone a complex history of aqueous and thermal alteration and offer crucial insights into early outer solar system conditions. In this study, we evaluate thermal infrared (TIR) reflectance spectra of three CY chondrites. We observe a broad spectral plateau near 10 μm, a spectral signature that has been observed in remote observations of some primitive, low-albedo asteroids, including Jupiter Trojans. We compare our data to CY emissivity spectra, spectra of Fe-sulfide and olivine mixtures, and remote Jupiter Trojan observations and establish the plateau and low albedo are a result of a high content of fine-particulate Fe-sulfide of these meteorites. We therefore suggest that D- and P-type asteroids, like Jupiter's Trojan asteroids, could have a high abundance of Fe sulfide on their surfaces as a potential result of aqueous alteration followed by dehydration, shedding light on the processes shaping the outer solar system.

Unified Astronomy Thesaurus concepts: Meteorites (1038); Carbonaceous chondrites (200); Asteroids (72); Jupiter trojans (874); Infrared spectroscopy (2285)

1. Introduction

Carbonaceous chondrite meteorites are samples of primitive asteroids that can be used to investigate conditions in the early solar system. A suite of ungrouped carbonaceous chondrites including Yamato (Y-) 86720, Y-86789 and Belgica (B-) 7904 (hereafter "CY" chondrites) have some chemical similarities to "Ivuna-like" (CI) and "Mighei-like" (CM) chondrites but record distinct alteration events, with extensive aqueous alteration producing a mineralogy dominated by phyllosilicates, Fe sulfides, carbonates, and magnetite, followed by short-term (>1000 days) thermal metamorphism at temperatures >500 °C that dehydrated phyllosilicates and caused recrystallization into fine-grained secondary anhydrous silicates (Y. Ikeda 1992; A. J. King et al. 2019; D. L. Schrader et al. 2025). Some CY meteorites retain primary Mg-rich silicates that survived aqueous alteration. A characteristic property of the CY chondrites is their high Fe-sulfide abundance (~15–30 vol.%), reflecting a different starting mineralogy and/or alteration history to other carbonaceous chondrite groups (Y. Ikeda 1992; T. Nakamura 2005; A. J. King et al. 2015, 2019; M. Suttle et al. 2023). Understanding the origin and evolution of the CY chondrites is therefore critical to comprehending aqueous and thermal processing in the early solar system.

A key question is how the CY chondrites are related to primitive solar system bodies. Based on their spectral characteristics, they have been linked to the active B-type asteroid (3200) Phaethon (E. MacLennan & M. Granvik 2024). H. Bates et al. (2021) presented near-infrared reflectance and thermal infrared (NIR-TIR; 2–50 μm) emissivity spectra of the CY chondrites collected under ambient and simulated asteroid environment (SAE) conditions, providing a new dataset for comparison with remote observations. The CY emissivity spectra show a unique feature near 10 μm (H. Bates et al. 2021), which is qualitatively reminiscent of the 10 μm "plateau" observed in some primitive asteroid spectra, including low-albedo asteroids and the Jupiter Trojan asteroids (hereafter "Trojans"). Trojans are trapped in stable Lagrange points in Jupiter's orbit at 5.2 au but are hypothesized to have formed in the primordial Kuiper Belt (H. F. Levison et al. 2009). They may represent some of the most primitive bodies in the solar system (H. F. Levison et al. 1997; A. Morbidelli et al. 2005). Most of the Trojans are classified as P- and D-type asteroids (F. DeMeo & B. Carry 2013), with some bodies of this spectral type also observed in the main asteroid belt, thought to have been emplaced there via dynamical changes in the early solar system (H. F. Levison et al. 2009). Evaluating the spectral similarity between CY chondrites, Trojans, and other P- and D-type asteroids in the TIR is critical as it may suggest a compositional relationship and might provide important details on the evolution of the protoplanetary disk where the Trojans accreted.

1.1. The 10 μm Plateau

The 10 μm plateau observed in the spectra of some primitive asteroids is an emission maxima between 9 and 12 μm and can be a variety of shapes from trapezoidal to triangular (J. Emery et al. 2006; A. C. Martin & J. P. Emery 2023; O. A. Humes et al. 2024). P- and D-type asteroids are among the lowest-albedo bodies in the solar system, with visible and near-infrared (VNIR; 0.4 to ~5 μm) spectra that exhibit either red

or less-red slopes and few diagnostic absorption features. While originally thought to be due to the presence of extensive organic material, these characteristics can be explained by the presence of anhydrous silicates mixed with spectrally neutral materials (Y. R. Fernández et al. 2003; J. Emery & R. Brown 2004; J. P. Emery et al. 2010; B. Yang & D. Jewitt 2011; I. Wong et al. 2024). Notably, D-type Trojans have VNIR spectra comparable to comets (D. C. Jewitt & J. X. Luu 1990; M. S. Kelley et al. 2017) and TIR spectra similar to cometary comae (J. Stansberry et al. 2004; J. Emery et al. 2006). Although Trojans lack comae (D. Perna et al. 2018), the similarity to comet spectra does suggest similar physical and/or compositional characteristics. As such, the 10 μm plateaus for the Trojans have been attributed to high-porosity, fine-particulate regolith (V. C. Lowry et al. 2022). This suggested physical structure may also be relevant for P- and D-type asteroids outside the Trojan population (O. A. Humes et al. 2024). Scenarios include a "fairy-castle" structure whereby sublimation of subsurface volatiles resulted in lofting and subsequent falling of dust onto surfaces (J. Emery et al. 2006) or surfaces covered in fine-particulate silicates suspended in salt lag deposits (B. Yang et al. 2013). The former scenario is favored, as salt has not been identified on Trojans and would result in higher albedos than observed (M. Izawa et al. 2021). Previous studies have recreated complex 10 μm spectral features by mixing powdered minerals and meteorites with potassium bromide (KBr; a TIR transparent material) that acts a proxy to simulate the postulated high-porosity regoliths (P. Vernazza et al. 2012, 2013; A. Martin et al. 2022, 2023; L. D. Dausend et al. 2025). Though spectra of KBr-diluted samples are better spectral analogs than undiluted material, they are not a perfect match. The use of KBr increases the albedo of the samples (high reflectance, reduced emissivity) over the same wavelengths where low-albedo asteroids show high emissivity.

Efforts to find appropriate compositional analogs from meteorite collections that can explain the 10 μm spectral features seen in TIR asteroid spectra have been limited. Porous (>80% void space) mixtures of amorphous and crystalline anhydrous silicates replicate the plateau observed in the Trojan spectra, but no appropriate natural analogs have been identified (A. Martin et al. 2022, 2023; A. C. Martin & J. P. Emery 2023), partly due to difficulties in replicating the appropriate near-surface conditions of these bodies. Currently, the meteorites providing the best spectral match to the 10 μm plateaus are the anhydrous "Ornans-like" (CO) and "Vigarano-like" (CV) carbonaceous chondrites (J. Emery et al. 2006; P. Vernazza et al. 2012), but the meteorite plateaus extend to longer wavelengths than those for the asteroids (J. Emery et al. 2006). The ungrouped C2 meteorite Tagish Lake has been discussed in the context of D-type asteroids, but inspection of its spectra reveals the Trojans in particular are too red to have a similar composition. Additionally, their mid-infrared (MIR) spectra are not a good match (J. Emery et al. 2006). The D-type asteroid Haidea, however, does appear to have a comparable spectrum to Tagish Lake (P. Vernazza et al. 2013). P. Vernazza et al. (2015) reported a good match between the TIR spectra of D-type asteroids and porous chondritic olivine- and pyroxene-rich interplanetary dust particles (CP-IDPs). These primitive particles contain 20–50 vol.% crystalline silicates as well as a high abundance of Fe sulfides (~40 vol.%) (J. Bradley 2014).

Recent investigations have shown reflectance spectra of physical mixtures of forsteritic olivine and Fe sulfide can replicate a 10 μm plateau (R. Sultana et al. 2023). As such, we present diffuse TIR (7–25 μm) reflectance spectra of three CY chondrites that show a high abundance of Fe sulfide and compare these datasets to both the TIR emissivity spectra collected by H. Bates et al. (2021) and the spectra of physical mixtures of forsterite and Fe sulfides measured by R. Sultana et al. (2023) in order to establish the cause of the 10 μm plateaus in CY chondrite spectra. We also compare the emissivity and reflectance CY chondrite spectra to remote observations of D- and P-type asteroids both in the Trojan population and elsewhere in the solar system and discuss whether they could have a CY-like composition.

2. Materials and Methods

2.1. Samples

We investigated the carbonaceous chondrites B-7904, Y-86720, and its pair Y-86789 (K. Matsuoka et al. 1996; A. J. King et al. 2019). Following near-complete aqueous alteration, Y-86720 and Y-86789 experienced thermal metamorphism at temperatures >700 °C and have been classified as CY2, H:IV chondrites by M. Suttle et al. (2023) and as stage IV heated CM chondrites by D. L. Schrader et al. (2025). The alteration history of B-7904 is similar, although it also contains primary, forsteritic olivine, indicating that prior to metamorphism at >700 °C, it underwent a lower degree of aqueous alteration than Y-86720 and Y-86789. It is also a CY2, H:IV in the M. Suttle et al. (2023) classification and a stage IV heated CM in the D. L. Schrader et al. (2025) system. As mentioned previously, for the purposes of this paper, we will refer to these samples as CY chondrites.

The bulk mineralogy of Y-86720 and Y-86789 is ~60 vol.% secondary olivine (Fo#70-80), ~8 vol.% pyroxene, ~32 vol.% Fe-sulfide, and ~3 vol.% metal; B-7904 contains ~25 vol.% primary olivine, ~50 vol.% secondary olivine (Fo#60-70), ~15 vol.% Fe sulfide, 2 vol.% carbonates, and ~2 vol.% metal (H. Bates et al. 2021). H. Bates et al. (2021) presented TIR emissivity spectra of Y-86720, Y-86789, and B-7904 collected in the Planetary Analog Surface Chamber for Asteroid and Lunar Environments (PASCALE; K. Donaldson Hanna et al. 2021) under ambient and SAE conditions. Here, we have acquired diffuse TIR reflectance spectra for the same subsamples as H. Bates et al. (2021). As the exact same subsamples were used, any spectral differences can be tied to the measurement method, so we can evaluate the differences between reflectance and emissivity techniques and test whether reflectance can be used as an appropriate proxy for emissivity. Measurements on the same subsamples of each meteorite will reduce meteorite heterogeneity effects: for example, the Winchcombe CM chondrite shows a variety of petrologic types (M. D. Suttle et al. 2024). Collecting spectra from a subsample of a meteorite, followed by collecting spectra on a different subsample of the same meteorite that may show a different petrologic type, would therefore introduce unreliability, resulting in a lower confidence in tying spectral features to compositional parameters.

2.2. Diffuse TIR Reflectance Spectral Measurements

TIR reflectance measurements were obtained using a Bruker VERTEX 70v Fourier Transform Infrared spectrometer with a

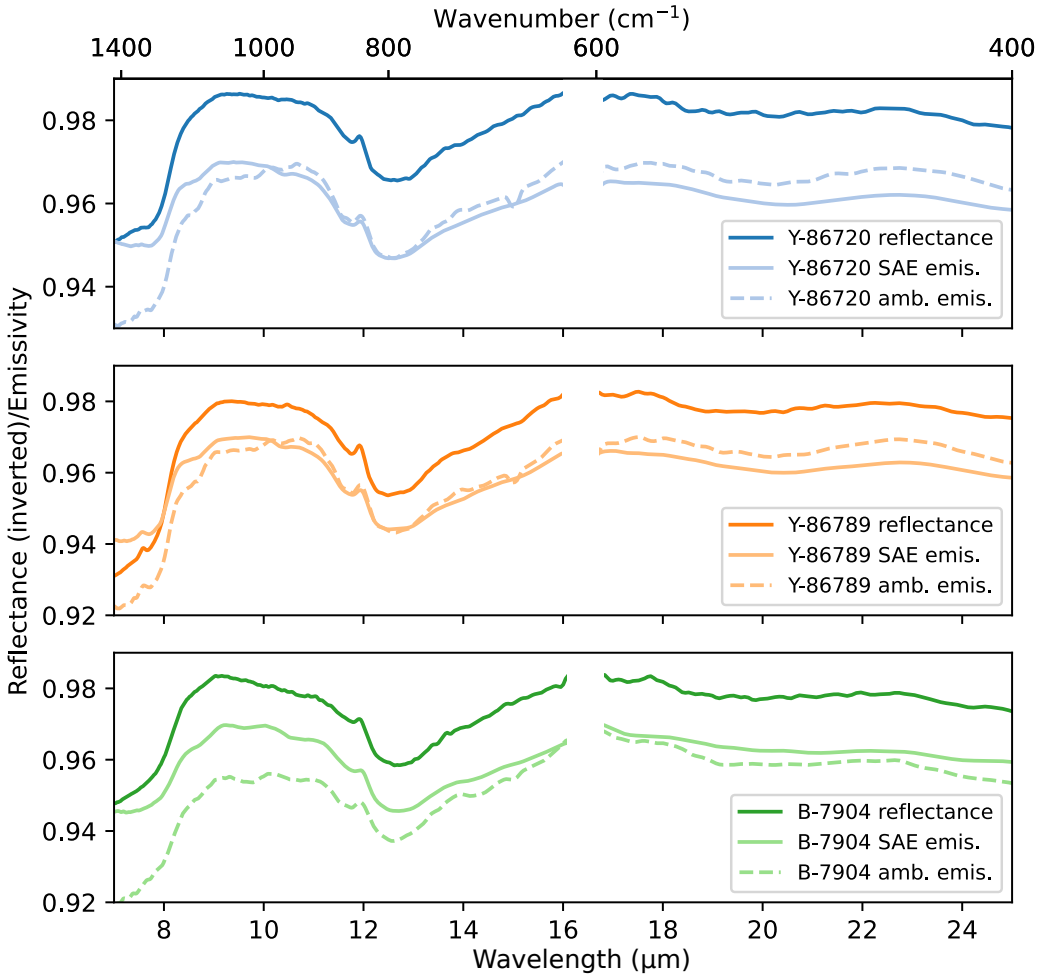

Figure 1. Reflectance spectra of Y-86720, Y-86789, and B-7904. Also included are the SAE and ambient emissivity measurements from H. Bates et al. (2021). Each emissivity spectrum is offset by −0.03. Gaps in the spectra near 16 μm are a region of low signal-to-noise due to low beam splitter throughput.

Specac Selector diffuse reflectance accessory at the Planetary Spectroscopy Facility at the University of Oxford. Approximately 200 mg of the powdered (particle size <35 μm) meteorite samples were loosely packed in stainless steel sample cups and the surfaces gently leveled by scraping any excess material off with a spatula. All observations were obtained under vacuum (~2 hPa) at a spectral resolution of 4 cm^{-1}, and the resulting spectra were the average of 250 scans. A wide-range mid- to far-IR (MIR-FIR) beam splitter and room temperature deuterated L-alanine doped triglycine sulfate (RT-DLaTGS) detector were used to measure the TIR reflectance. The Bruker FTIR, beam splitter, and detector is the same system used to measure the emissivity spectra in H. Bates et al. (2021). A diffuse gold standard was used as a calibration reference, and reflectance was calculated by ratioing the sample spectra to a gold spectrum. Three spectra were taken for each sample and then averaged to give the final spectrum.

3. Results

Figure 1 shows the TIR reflectance and emissivity spectra of the CY chondrites. Unlike diffuse reflectance and emissivity spectra of CM chondrites (H. Bates et al. 2020, 2021; K. Donaldson Hanna et al. 2021), the CY spectra show a broad plateau feature between ~9 and ~11 μm and no easily identifiable Christiansen features (CFs). Reflectance spectra for all CY chondrites also show minima near 11.78 μm, followed by a sharp peak at 11.92 μm, the latter of which is consistent with features observed in Fo#70-80 olivine spectra (C. Koike et al. 2003). The CY spectra also show transparency features between 12.49 and 12.69 μm and broad minima at 19.51–20.26 μm. These ~20 μm features are consistent with the spectra of Fo#80 olivine, although multiple individual olivine features bands 5a, 6, and 7 (V. E. Hamilton 2010) and bands 8 and 9 (M. D. Lane et al. 2011) are being averaged out to create a single wider feature, due to the poorly crystalline nature of this recrystallized olivine. These olivine features are consistent with the bulk mineralogy of these samples: the CYs contain abundant Fo#70-80 olivine (A. J. King et al. 2019; H. Bates et al. 2021).

In addition, we calculated the positions of the vibrational bands immediately adjacent to the plateau, spectral contrast, width, slope, skew, and continuum-removed peak position of the 10 μm plateau, using the methodology established by A. C. Martin & J. P. Emery (2023). We also calculated these parameters for the H. Bates et al. (2021) emissivity spectra. These results are shown in Table 1. Briefly, we generated 10,000 synthetic spectra for both the reflectance and emissivity spectra using the uncertainty associated with each spectral value: at each wavelength, a random spectral value within the uncertainty bounds was selected. For each 10 μm plateau in each spectrum, we used the positions of vibrational features on either side as the "plateau start" and "plateau end," with the

Table 1
Calculated Parameters for the 10 μm Plateau in the Reflectance and Emissivity Spectra of the CY Chondrites

	Plateau Start (μm)	Plateau End (μm)	CR[a] Peak Position (μm)	Spectral Contrast (%)	Width (μm)	Slope (μm^{-1})	Skew[b] (%)
Y-86720	7.55 ± 0.08	12.65 ± 0.08	9.44 ± 0.04	2.97 ± 0.02	5.11 ± 0.08	0.002 ± 0.0001	−12.89 ± 1.01
Y-86720 (amb. emis.)	7.62 ± 0.08	12.59 ± 0.08	9.62 ± 0.52	3.14 ± 0.06	4.97 ± 0.08	0.003 ± 0.001	−9.51 ± 10.44
Y-86720 (SAE emis.)	7.67 ± 0.19	12.56 ± 0.19	9.64 ± 0.23	2.69 ± 0.08	4.89 ± 0.19	−0.001 ± 0.0002	−9.49 ± 4.79
Y-86789	7.66 ± 0.05	12.49 ± 0.05	9.33 ± 0.01	3.90 ± 0.02	4.85 ± 0.05	0.003 ± 0.0001	−15.38 ± 0.05
Y-86789 (amb. emis.)	7.64 ± 0.12	12.62 ± 0.12	9.38 ± 0.46	3.80 ± 0.06	4.99 ± 0.12	0.003 ± 0.0001	−15.24 ± 9.07
Y-86789 (SAE emis.)	7.67 ± 0.24	12.59 ± 0.24	9.57 ± 0.31	3.99 ± 0.18	4.92 ± 0.24	0.001 ± 0.0003	−11.71 ± 6.37
B-7904	6.63 ± 0.08	12.71 ± 0.08	9.16 ± 0.01	3.48 ± 0.02	6.07 ± 0.08	0.002 ± 0.0001	−8.23 ± 0.59
B-7904 (amb. emis.)	7.54 ± 0.09	12.59 ± 0.09	9.28 ± 0.11	3.06 ± 0.08	5.04 ± 0.09	0.003 ± 0.0001	−15.85 ± 2.11
B-7904 (SAE emis.)	7.62 ± 0.19	12.68 ± 0.19	9.48 ± 0.32	3.36 ± 0.15	5.05 ± 0.19	0.001 ± 0.0003	−13.20 ± 6.15
Hektor (D)	8.50 ± 0.04	12.50 ± 0.02	10.13 ± 0.09	11.77 ± 0.81	4.00 ± 0.04	0.005 ± 0.001	14.25 ± 0.23
Agamemnon (D)	8.22 ± 0.13	12.42 ± 0.04	9.23 ± 0.23	11.75 ± 1.50	4.20 ± 0.11	0.012 ± 0.001	15.00 ± 1.52
Aneas (D)	8.00 ± 0.16	12.56 ± 0.01	10.13 ± 0.05	10.36 ± 2.24	4.56 ± 0.16	0.009 ± 0.001	−0.22 ± 1.23
Cybele (P/Xc)	7.90 ± 0.10	12.27 ± 0.07	9.68 ± 0.04	5.8 ± 0.6	4.37 ± 0.12	0.001 ± 0.002	−9 ± 7
Sylvia (P/X)	7.80 ± 0.04	12.03 ± 0.11	9.68 ± 0.14	6.1 ± 0.6	4.23 ± 0.12	0.003 ± 0.001	−6 ± 10
Tirza (DU/D)	7.80 ± 0.10	12.67 ± 0.10	9.81 ± 0.15	12 ± 2.0	4.87 ± 0.14	0.005 ± 0.005	−9 ± 9
Justitia (Ld/IR-RR[c])	7.85 ± 0.02	12.82 ± 0.07	9.64 ± 0.15	5.1 ± 0.8	4.87 ± 0.07	0.002 ± 0.001	−14 ± 1
Lacadiera (D/Xk)	7.63 ± 0.08	11.97 ± 0.11	9.63 ± 0.17	4.6 ± 0.9	4.34 ± 0.14	0.001 ± 0.003	−4 ± 11
Haidea (D)	8.18 ± 0.05	12.18 ± 0.04	9.26 ± 0.02	6.5 ± 2.1	3.90 ± 0.06	0.004 ± 0.005	−25 ± 6
Hidalgo (D)	7.41 ± 0.06	12.28 ± 0.06	9.81 ± 0.17	11 ± 0.7	4.87 ± 0.08	0.009 ± 0.002	−1 ± 8
Libya (P)	7.74 ± 0.03	12.30 ± 0.04	9.61 ± 0.26	6.7 ± 0.7	4.56 ± 0.05	0.010 ± 0.002	−9 ± 14
Kalahari (D/L)	7.99 ± 0.04	12.27 ± 0.05	9.43 ± 0.12	7.3 ± 1.8	4.63 ± 0.05	0.014 ± 0.004	−11 ± 7

Notes. Also included are the same parameters calculated by A. C. Martin & J. P. Emery (2023) for the Trojan asteroids Hektor, Agamemnon, and Aneas and for a suite of Cybele group asteroids, main-belt asteroids, and one Centaur (Hidalgo) calculated by O. A. Humes et al. (2024). Taxonomic groups are given as Tholen/SMASSII classifications from C. Neese (2010) in parentheses following the asteroid name.

[a] CR: continuum removed.

[b] The skew values reported by O. A. Humes et al. (2024) were linearly converted to the A. C. Martin & J. P. Emery (2023) definition by subtracting 0.5 and converting to a percent value. Uncertainties were propagated unchanged. We note that the skew values from O. A. Humes et al. (2024) are reported to fewer significant figures, reflecting the precision of the original published data.

[c] Justitia's "Intermediate Red—Very Red" taxonomic classification comes from the Tholen/TNO classification scheme. (S. Hasegawa et al. 2021). Its Ld classification is similar to a D classification but shows a flattening of reflectance toward 1 μm in comparison to a D type, which shows a continued increase of reflectance in that range.

linear slope between the two points taken as the continuum and the distance between as the width. These bounding vibrational features were determined using the `SciPy.signal.argrelextrema` function. We normalized the spectra by dividing by the linear continuum and took the maximum value (using the `numpy.argmax` function) in the resulting continuum-removed spectra as the continuum-removed peak position and the difference between this peak and the continuum as the spectral contrast. The skew is the difference between the continuum-removed peak and the midway point of the plateau (i.e., half the width) and is represented as a percentage of the width. Negative values indicates the plateau leans to shorter wavelengths and vice versa for positive skew values. All the 10 μm plateaus in the meteorite spectra show a negative skew, although the skews in the emissivity spectra have larger errors (±2.11 to ±10.44). This is because the plateaus in these data are relatively flat, so the slight variation between the synthetic spectra results in reasonably large variations in continuum-removed peak positions.

4. Discussion

4.1. Comparing Reflectance and Emissivity Spectral Measurements

The reflectance spectra of Y-86720 and Y-86789 are similar, with spectral features identified at similar wavelengths, which is expected as the two meteorites are likely paired (K. Matsuoka et al. 1996). The reflectance spectrum of B-7904 differs slightly, as its plateau feature is slightly broader and starts at a shorter wavelength, likely due to a crystalline forsteritic component in this meteorite, the spectra of which show features at shorter wavelengths (V. E. Hamilton 2010). B-7904 contains a higher primary forsterite component than the Y-86720 and Y-86789 meteorites due to its lower extent of aqueous alteration prior to its thermal metamorphism, so this mineral component escaped alteration to phyllosilicate. Y-86720 and Y-86789 contain no primary forsterite as it was entirely altered to phyllosilicates during aqueous alteration, before being decomposed and recrystallized as Fo#70-80 olivine (M. Suttle et al. 2023). Differences between the emissivity spectra of B-7904, Y-86720, and Y-86789 are described in H. Bates et al. (2021); here, we focus on differences between the emissivity and reflectance spectra. As the same aliquots were used to collect both reflectance and emissivity spectra, any differences result from the collection environment rather than meteorite heterogeneity. For each meteorite, both the emissivity and reflectance spectra show plateau features between ∼9 and ∼11 μm and transparency and vibrational features in similar positions. However, compared to their reflectance spectra, the emissivity spectra have more individual vibrational features that can be distinguished in the plateau, likely because they show higher signal-to-noise from the samples being heated and spectral

emission dominating spectral flux over reflectance at wavelengths greater than 5 μm (A. Rivkin et al. 2005).

There is also a difference in the spectral slope, particularly when considering the "top" of the 10 μm plateau in the ambient emissivity spectra compared to that in the reflectance spectra. This may be a result of the removal of a single-temperature Planck function during calibration of the emissivity spectra (J. W. Salisbury et al. 1991; K. Donaldson Hanna et al. 2021); however, we note that the calculated slope across the whole of the plateau feature does not vary significantly between the two methodologies (Table 1). This suggests the variation is due to differences in the shapes of vibrational features, which is likely due to the difference in experimental geometry. Emissivity spectra are often approximated from reflectance spectra using Kirchhoff's law: emissivity = 1 – reflectance (F. E. Nicodemus 1965); however, this is only strictly valid for hemispherical reflectance measurements and for samples in thermodynamic equilibrium with their environment (J. W. Salisbury et al. 1991; P. R. Christensen & S. T. Harrison 1993; J. Salisbury 1993). Reflectance is highly dependent on the experimental system geometry, and although diffuse reflectance of powders is considered appropriate at approximating emission, the diffuse setup has incident and reflected light at set angles. Previous studies have shown that varying these angles can change the positions and shapes of spectral features (J. Gradie & J. Veverka 1980; V. Reddy et al. 2012), and the positional offsets we observe are consistent with the literature (A. C. Martin et al. 2025). It is clear from our results that diffuse reflectance is effective at approximating emissivity as long as positional offsets are considered; however, differences in shapes of vibrational features can be expected.

4.1.1. What Causes the 10 μm Plateau in the CY Spectra?

The reflectance and emissivity spectra of the CY chondrites can contribute to our understanding of the 10 μm plateau on the surfaces of low-albedo asteroids. Recently, R. Sultana et al. (2023) showed that mixing submicron particulate olivine (Fo# >94) with Fe sulfide (55 vol.% troilite, 45 vol.% pyrrhotite) produces a similar 10 μm plateau in reflectance spectra as observed with olivine/KBr mixtures. R. Sultana et al. (2023) suggested that the opaque Fe-sulfide grains separate and isolate silicate grains, resulting in photons being able to escape the sample after interacting with a single silicate particle, similar to the effect of mixing silicate with an infrared-transparent material to simulate porosity. This produces emissivity spectra that resemble silicates measured in transmission and look like the 10 μm plateau. Crucially, the overall reflectances of the olivine/Fe-sulfide mixtures are lower than olivine/KBr mixtures and thus potentially more comparable with remote observations of low-albedo asteroids: the albedos for the 60:40 and 70:30 olivine/Fe-sulfide mixtures are 0.077 and 0.066, respectively (R. Sultana et al. 2023), and D-type asteroids have an average albedo of 0.098 (F. DeMeo & B. Carry 2013).

We propose that the CY chondrites, which contain ~15–30 vol.% Fe sulfide, are natural examples of the phenomenon observed by R. Sultana et al. (2023). CM chondrites typically have Fe-sulfide abundances of 1–5 vol.%, CV chondrites 2–8 vol.%, and COs 2–3 vol.% (C. Alexander et al. 2018; K. Howard et al. 2010, 2015). Sulfide grains in the CYs range from <1 to >250 μm in size (M. Suttle et al. 2023); however, during sample preparation, we ground our samples to <35 μm sized particles.

Figure 2 shows the reflectance spectra of Y-86720 (paired with Y-86789) and B-7904 and olivine/Fe-sulfide mixtures from R. Sultana et al. (2023). We note that the particle sizes of our samples (<35 μm) differ from the R. Sultana et al. (2023) samples (<1 μm). This is unlikely to change the positions of most spectral features, although it might affect spectral contrast and the overall shape of the plateau (D. C. Cantillo et al. 2023), so we will focus on comparing feature positions. The plateaus observed in the meteorite spectra are clearly broader than those observed in the olivine/Fe-sulfide spectra. The shorter wavelength "edge" of the plateau for both Y-86720 and B-7904 matches reasonably well with the 90:10 and 80:20 mixtures; however, these ratios are inconsistent with the mineralogy of the CY samples, which typically contain olivine in lower abundances (<75 vol.%; H. Bates et al. 2021). When compared to the spectra of the 70:30 and 60:40 olivine/Fe-sulfide mixtures, the plateau in the CY chondrite spectra extend to shorter wavelengths than expected. This is likely due to the CY chondrites containing relatively abundant (~5–9 vol.%) pyroxene. Pyroxene shows resonance features near 9.2–9.3 μm (H. Chihara et al. 2002), and its presence might explain the shorter wavelength edge observed in the plateau of the CY chondrite spectra. This pyroxene interpretation is consistent with conclusions from A. Martin et al. (2023), who attributed features near 9.2 μm in the plateau observed in the spectra of some Trojans to Mg-rich pyroxene, and with observations by O. A. Humes et al. (2024) who showed in mixtures of olivine and pyroxene that spectra of those with higher pyroxene abundances have 10 μm plateau, which skews to shorter wavelengths. In addition to this shorter wavelength edge, the plateau feature observed in the CY chondrite spectra extends to longer wavelengths than in the spectra of the analog mixtures, which may be due to the variety of less Mg-rich olivine chemistries present in the CYs compared to the Fo# >94 olivine present in the mixtures; for example, changing olivine chemistry from Fo# 91 to Fo# 66 results in a shift of a spectral feature in the plateau range from 10.5 to 10.8 μm (V. E. Hamilton 2010). Pyroxene also has a peak near 11.50 μm (H. Chihara et al. 2002), and the combined effects of the pyroxene component and the less Mg-rich olivine could lengthen the plateau and shift the 11.78 μm feature to longer wavelengths than observed in the analog mixture spectra. Other differences between the CY chondrite and analog spectra include the longer wavelengths of the 20 μm minima and the transparency feature in the meteorite spectra. Again, the position of these minima can be explained by the Fe-rich composition of secondary olivine in the CY chondrites resulting in features at longer wavelengths.

4.1.2. Could the CY Chondrites Be Samples of Trojans?

Table 1 shows the parameters calculated for the 10 μm plateau observed in the meteorite spectra and in the spectra of the Trojan asteroids Hektor, Agamemnon, and Aneas. Also included are the same parameters calculated from the spectra of a suite of P- and D-type asteroids outside of Jupiter's orbit believed to have originated from the same solar system reservoir (O. A. Humes et al. 2024). Figure 3 demonstrates the similarity of the CY chondrite spectra and remote observations of the Trojan asteroids. In the previous section, we argued that the CY spectra are natural examples of the phenomenon

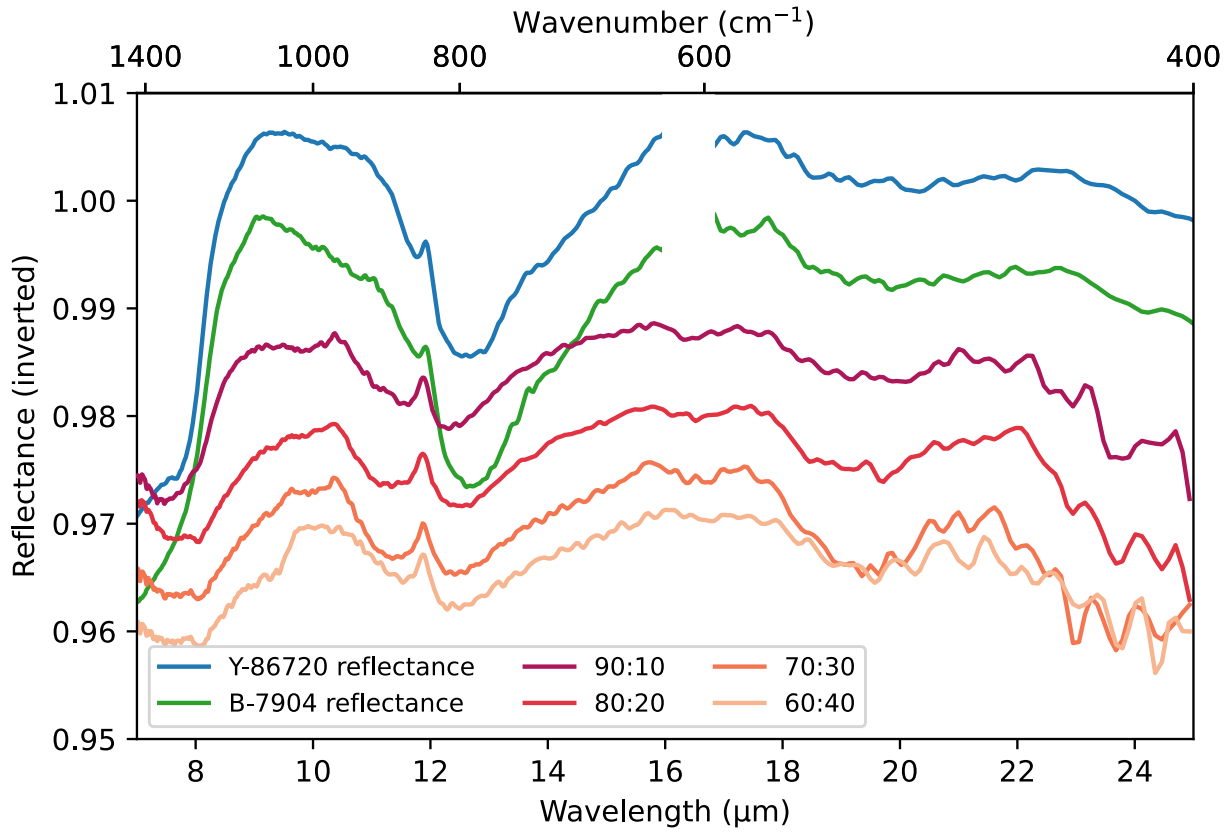

Figure 2. The reflectance spectra of Y-86720 (blue) and B-7904 (green), with the reflectance spectra of olivine/Fe-sulfide mixtures from R. Sultana et al. (2023). Gaps in the meteorite reflectance spectra near 16 μm are a region of low signal-to-noise due to low beam splitter throughput.

described by R. Sultana et al. (2023), whereby Fe sulfides disperse fine-particulate silicate grains, resulting in 10 μm plateau features. We offer this additional compositional explanation for the 10 μm plateau observed in the spectra of the Trojans and related dark, primitive asteroids. If present, a high abundance of Fe sulfides and a CY-like mineralogy could suggest a complex aqueous and thermal alteration history of the materials on their surfaces.

There are key differences between the remote asteroid and laboratory meteorite spectra. The 10 μm plateaus in the CY chondrite spectra start at shorter wavelengths than those observed for the Trojans, resulting in a larger overall plateau width (Table 1). The plateaus in the meteorite spectra also show a shoulder (particularly obvious in the emissivity spectra) near 8.3–8.5 μm. H. Bates et al. (2021) linked this shoulder to the CF of pyroxene, but this is evidently suppressed when measuring reflectance. A. C. Martin & J. P. Emery (2023) suggested the presence of an additional unidentified material (i.e., not olivine or pyroxene) on the Trojan surfaces that suppresses features at shorter wavelengths, as they were unable to recreate the Trojan 10 μm plateau with silicate mixtures alone. If that suggestion is correct, this suppressing component is absent in the CY chondrites, potentially also explaining why the skew of the plateaus in the CY spectra are all toward shorter wavelengths, in contrast to the longer wavelength skew of the Trojan spectra, and the continuum-removed peak positions are also at shorter wavelengths in the meteorite spectra (Table 1). In contrast, the parameters calculated from the other D-/P-type asteroid spectra show a more comparable plateau start, continuum-removed peak position, width, and skew to the meteorite spectra, and the difference in these asteroid parameters in comparison to the Trojan spectra was noted by O. A. Humes et al. (2024) as confirming the presence of an unknown physical mechanism responsible for suppressing features at shorter wavelengths in the Trojan spectra. This may point to this mechanism being related to the Trojans' current location in the solar system.

The Trojan spectra additionally show minima near 15 μm that is absent from most of the meteorite spectra. The absence of this feature may also suggest the presence of an unidentified material on the Trojans that is absent from the CYs. However, we note that a subtle feature near 15 μm can be observed in the meteorite ambient emissivity spectra. H. Bates et al. (2021) found spectral features disappeared and appeared when measuring ambient and SAE emissivity, thus indicating some mineral phases change the way they emit with a change in environmental conditions. It may be that the 15 μm minimum is a real compositional feature, and due to the reasons suggested earlier (higher signal-to-noise for emissivity spectra), this feature is not observable in the reflectance spectra. We also note that an excess emission at the end of the Short-Low 1 mode of the Spitzer Space Telescope can potentially lead to a "14 μm teardrop" feature in asteroid spectra, which makes comparisons even more challenging (Spitzer Science Center, 2011).

Another difference between the asteroid and laboratory spectra is all meteorite spectra show transparency features (minima) near 12.5 μm, which are a result the fine-particulate size of the samples. Additionally, the spectral contrast of the 10 μm plateau in the meteorite spectra is generally reduced compared to the remote observations, similar to findings by

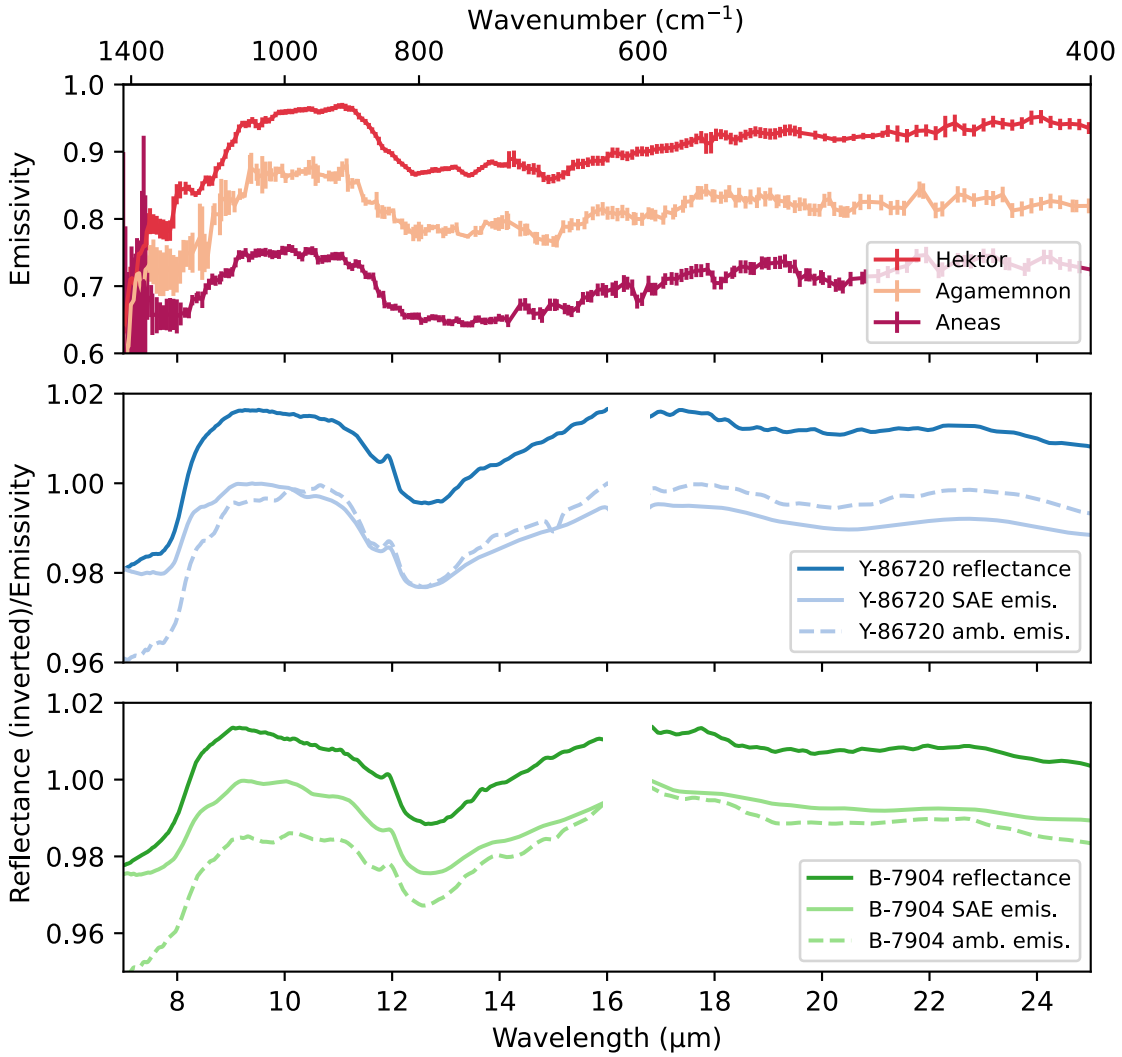

Figure 3. TIR spectra of Trojans 624 Hektor, 911 Agamemnon, and 1172 Aneas (J. Emery et al. 2006), compared to the inverted reflectance and emissivity of Y-86720 and B-7904. Gaps in the meteorite spectra near 16 μm are a region of low signal-to-noise due to low beam splitter throughput.

R. Sultana et al. (2023), although they are within error of some of the spectral contrasts established for the "less-red" Trojan asteroid spectra in A. C. Martin & J. P. Emery (2023). We propose that the cause of these differences stems from differences in porosity between the laboratory samples and asteroid surfaces. We can estimate the porosity of our samples as prepared in the sample cup as between 70% and 80% using the volume of the sample cup, mass of sample required to fill it, and estimated density of the CY chondrites (carbonaceous chondrite bulk densities tend to range between 2.25 and 3 g cm^{-3}, G. Consolmagno et al. 2008). The surfaces of the Trojans are predicted to have regolith porosities of >80%, and increased porosity causes increases in spectral contrast (V. C. Lowry et al. 2022; A. Martin et al. 2022, 2023; A. C. Martin & J. P. Emery 2023). While the Fe-sulfide content produces the 10 μm feature observed, it does not fully reproduce the estimated porosity on the asteroid surfaces, likely resulting in the observed differences.

It is clear the mineralogy of the CY chondrites is not a perfect match to the composition of the Trojan and other D-/P-type asteroid surfaces discussed here, based on differences between laboratory and remote spectra. This is consistent with results from A. Martin et al. (2023), who identified spectral features in Hektor, Agamemnon, and Aneas spectra associated with Mg-rich forsterite and enstatite, and weak features associated with fayalite in all. Although similar, this mineralogy slightly differs from that of bulk CY chondrites. What the CY chondrite spectra presented here do suggest, though, is that while the asteroids discussed here may not be the source of the CY chondrites, their surfaces may have abundant (∼15–30 vol.%) fine-particulate opaque material, such as Fe sulfides. This conclusion is consistent with Shkuratov modeling of D-type asteroids both in the Trojan swarm and elsewhere in the solar system, which show a sulfide abundance of 7%–25% (G. M. Gartrelle et al. 2021). When we compare our data to the larger Trojan spectral dataset presented in A. C. Martin & J. P. Emery (2023), the differences between meteorite and asteroid spectra are similar, with the plateaus being wider and starting at shorter wavelengths in the meteorite spectra. There is some similarity in spectral contrasts of the meteorite and asteroid spectra, as previously mentioned, and the D-/P-type Trojan asteroid Diomedes has a continuum-removed peak position of 9.61 μm, a spectral contrast of 4.54%, and plateau width of 4.14 μm (A. C. Martin & J. P. Emery 2023), which are similar to the parameters measured in the meteorite spectra, indicating some

asteroids in the Trojan population may be more similar to the CY chondrites than others.

The bulk chemical and isotopic compositions of the CY chondrites indicate a potential affinity with the CM and CI chondrites, which are thought to have accreted with high water/rock ratios in the outer solar system (T. Hopp et al. 2022; D. L. Schrader et al. 2025). However, the high Fe-sulfide abundance is a distinct property of the CY chondrites and reflects their initial mineralogy and the extent to which they were modified by aqueous and thermal alteration on the parent body (A. J. King et al. 2019; M. Suttle et al. 2023). If Trojan and other D-/P-type asteroid surfaces do have high abundances of sulfides, they may share affinities with CY chondrites and may have experienced a similar processing of aqueous alteration and then partial dehydration by a thermal event(s). Dynamical simulations suggest the Trojans and D-/P-type asteroids elsewhere in the solar system are remnants of the primordial Kuiper Belt (A. Morbidelli et al. 2005; H. F. Levison et al. 2009; D. Nesvorný et al. 2013; F. E. DeMeo et al. 2014), in which they likely accreted anhydrous silicates, Fe metal, and volatile ices including H_2S (I. Wong & M. E. Brown 2016). Ices might have been melted by the heat from the decay of radiogenic elements (e.g., ^{26}Al), resulting in aqueous alteration within the interior of the bodies and producing phyllosilicates and Fe sulfides, as well as other mineral phases. On large planetesimals, outer crusts of unaltered, potentially icy, materials would have helped to retain heat produced from radioactive decay (R. E. Grimm & H. Y. McSween 1989; B. A. Cohen & R. F. Coker 2000; J. Palguta et al. 2010). Heating from solar radiation could have occurred during the inward migration of dark, primitive asteroids, with some ending up on highly elliptical orbits that brought them within <2 au of the early Sun (A. Morbidelli et al. 2005). This is consistent with the distribution of these dark D-/P-type asteroids throughout the solar system, as not all bodies would have migrated outwards following their inward travel, and some would have remained in the main asteroid belt (H. F. Levison et al. 2009; F. E. DeMeo et al. 2014). Alternatively, models show that collision probabilities within the Trojan population are orders of magnitude higher than in other destabilized primordial Kuiper Belt Object (KBO) populations (W. F. Bottke et al. 2023). A high impact rate in the Trojan population compared to the Kuiper Belt would remove the unaltered crusts, exposing an underlying aqueously altered mineralogy, which may have become dehydrated by further impacts, although this scenario does not explain the presence of 10 μm plateaus in the spectra of dark asteroids outside of this population.

There are several challenges to the hypothesis that the Trojans and other D-/P-type asteroids experienced significant processing. For example, impacts typically result in localized dehydration (T. Nakamura et al. 2022) and probably only occurred on some bodies, with signs of aqueous alteration likely recorded elsewhere in the population. Recent James Webb Space Telescope (JWST) spectra of some Trojans have features centered at 3 μm attributed to water ice or irradiation residues, but they do not show the characteristic sharp hydrated silicate feature at 2.7 μm (I. Wong et al. 2024). Observations of the asteroid Cybele have shown a similar feature at 3.1 μm (L. O'Rourke et al. 2020). We note that near-infrared (NIR) spectra of CY chondrites show a broad, bowl-like feature at slightly shorter wavelengths than that observed in the Trojan spectra, centered near 2.9 μm, also with no sharp 2.7 μm feature (H. Bates et al. 2021). This spectral shape is associated with dehydrated phyllosilicates and indicates processed phyllosilicates do not always show the typical hydrated silicate feature. In addition to this, more traditional signs of hydrated material on other primitive D-/P-type asteroids outside of the Trojan population are present: the spectrum of asteroid Justitia can be modeled by mixtures of anhydrous silicates and CM-like carbonaceous material (Harish et al. 2025); and the visible-NIR spectrum of Haidea is most similar to the spectrum of CM2 Cold Bokkeveld (F. Vilas & M. J. Gaffey 1989). Additionally, JWST spectra of Elara and Himalia, two of Jupiter's irregular satellites, show a sharp 2.7 μm feature, indicating the presence of ammoniated phyllosilicates, showing evidence for aqueous alteration products in populations thought to have a similar formation region to the Trojans (B. N. Sharkey et al. 2025).

Those asteroids considered here for which density has been determined have apparently low density, e.g., 1 g cm^{-3} for Hektor (F. Marchis et al. 2006; P. Lacerda & D. C. Jewitt 2007), and 1.3 g cm^{-3} for Sylvia (P. Vernazza et al. 2021). Hektor and Sylvia are both large bodies (110–120 km and 246–267 km, respectively (D. P. Cruikshank 1977; E. F. Tedesco et al. 2002; Y. R. Fernández et al. 2003; O. A. Humes et al. 2024) and thus are unlikely to be "rubble piles" of a larger parent planetesimal, although we do note that Sylvia has been described as a rubble pile elsewhere in the literature due to the fact it is part of a ternary asteroid system (F. Marchis et al. 2005). Instead, the low densities may suggest that the Hektor and Sylvia interiors have high macro porosity and/or contain abundant ices. However, aqueous alteration should have depleted ices in the asteroid interiors and lithified the rocky materials, resulting in densities more comparable to carbonaceous chondrites. A possible explanation is that these bodies, along with the other D-/P-type asteroids, accreted late, such that impacts (A. E. Rubin 2012) or solar radiation were the main heat sources driving aqueous alteration rather than radioactive decay. As impacts and solar radiation are both surface processes, this could have produced asteroids with unaltered, icy interiors surrounded by crusts of dehydrated material. Alternatively, surfaces were not dehydrated in situ, and material ejected from the surfaces was dehydrated during movement to the inner solar system. However, we note that a carbonate grain in the CY chondrite Y-980115 records an age of 4563 Myr (W. Fujiya et al. 2013), implying the CY parent body accreted early (i.e., <4 Myr after calcium- aluminum-rich inclusions formed).

Alternatively, rather than being CY-like, Trojans and other D-/P-type asteroids may be compositionally similar to CP-IDPs, which can contain abundant sulfides (up to $\sim$40 vol.%) that may have formed through gaseous sulfidization of preexisting FeNi metal grains in the solar nebula (J. Bradley 2014). In this model, the asteroids have an anhydrous mineralogy that did not experience any significant aqueous or thermal processing. This supports the identification of 10 μm plateau features on all observed Trojans and on a significant number of dark, primitive asteroids elsewhere in the solar system thus far. We anticipate that NASA's Lucy mission (H. F. Levison et al. 2021) will help to distinguish between the two scenarios proposed. If the visited Trojan surfaces were dehydrated, we would expect to see a variety of aqueous alteration and dehydration extents on different Trojans. If the surfaces were primitive and unaltered, we

would expect no evidence for hydration and spectral features that can be tied to primary silicates only.

5. Conclusions

The reflectance spectra of CY chondrites show features that are consistent with their mineralogy, including a broad 10 μm plateau that likely results from their high Fe-sulfide abundances and fine-particulate nature. We find that the shape of the 10 μm plateau for the CY chondrites is similar to those observed in TIR spectra of Jupiter Trojan and other dark, primitive D-/P-type asteroids, suggesting that they could have surfaces with high abundances of Fe sulfides. The mineralogy of the CY chondrites reflects extensive water–rock reactions followed by dehydration and recrystallization of phyllosilicates during short-lived metamorphism at >500 °C. Assuming they have a similar alteration history, our data support a model whereby D-/P-type asteroids accreted early and were aqueously altered in a primordial Kuiper Belt and then they, or material ejected from their surfaces, experienced solar radiation or high collisional rates resulting in dehydration before being emplaced in their current locations throughout the solar system. Alternatively, D-/P-type asteroids may be compositionally similar to CP-IDPs, which also contain high sulfide abundances. Future observations by JWST (J. P. Gardner et al. 2006), and potentially, NASA's Lucy mission (H. F. Levison et al. 2021), will be crucial to further understanding the formation and evolution of these objects and processes occurring in the outer solar system.

Acknowledgments

The authors thank the multiple reviewers who gave comments that greatly improved this paper. We would also like to acknowledge NIPR, Japan, for providing meteorites samples investigated in this study. This work was funded through the STFC Council grant 1860431 and UKRI grant MR/T020261/1.

ORCID iDs

Helena C. Bates https://orcid.org/0000-0002-0469-9483
Ashley J. King https://orcid.org/0000-0001-6113-5417
Kerri L. Donaldson Hanna https://orcid.org/0000-0001-5592-4292
Audrey C. Martin https://orcid.org/0000-0003-3402-1339
Joshua P. Emery https://orcid.org/0000-0001-9265-9475
Neil E. Bowles https://orcid.org/0000-0001-5400-1461
Sara S. Russell https://orcid.org/0000-0001-5531-7847

References

Alexander, C., Greenwood, R., Bowden, R., et al. 2018, A Multi-technique Search for the Most Primitive CO Chondrites, GeCoA, 221, 406
Bates, H., Donaldson Hanna, K., King, A., Bowles, N., & Russell, S. 2021, A Spectral Investigation of Aqueously and Thermally Altered CM, CM-An, and CY Chondrites under Simulated Asteroid Conditions for Comparison with OSIRIS-Rex and Hayabusa2 Observations, JGRE, 126, e2021JE006827
Bates, H., King, A., Donaldson Hanna, K., Bowles, N., & Russell, S. 2020, Linking Mineralogy and Spectroscopy of Highly Aqueously Altered CM and CI Carbonaceous Chondrites in Preparation for Primitive Asteroid Sample Return, M&PS, 55, 77
Bottke, W. F., Vokrouhlická, D., Marschall, R., et al. 2023, The Collisional Evolution of the Primordial Kuiper Belt, Its Destabilized Population, and the Trojan Asteroids, PSJ, 4, 168
Bradley, J. 2014, Early Solar Nebula Grains—Interplanetary Dust Particles, Meteorites and Cosmochemical Processes (Elsevier), 287
Cantillo, D. C., Reddy, V., Battle, A., et al. 2023, Grain Size Effects on UV–MIR (0.2–14 μm) Spectra of Carbonaceous Chondrite Groups, PSJ, 4, 177
Centre, S. S., Team, I. I., & Team, U. S. 2011, IRS Instrument Handbook Version 5.0, Spitzer Hertigate Archive Documentation, Tech. Rep., IPAC https://catcopy.ipac.caltech.edu/dois/doi.php?id=10.26131/IRSA487
Chihara, H., Koike, C., Tsuchiyama, A., Tachibana, S., & Sakamoto, D. 2002, Compositional Dependence of Infrared Absorption Spectra of Crystalline Silicates.I. Mg-Fe Pyroxenes, A&A, 391, 267
Christensen, P. R., & Harrison, S. T. 1993, Thermal Infrared Emission Spectroscopy of Natural Surfaces: Application to Desert Varnish Coatings on Rocks, JGRB, 98, 19819
Cohen, B. A., & Coker, R. F. 2000, Modeling of Liquid Water on CM Meteorite Parent Bodies and Implications for Amino Acid Racemization, Icar, 145, 369
Consolmagno, G., Britt, D., & Macke, R. 2008, The Significance of Meteorite Density and Porosity, Geoch, 68, 1
Cruikshank, D. P. 1977, Radii and Albedos of Four Trojan Asteroids and Jovian Satellites 6 and 7, Icar, 30, 224
Dausend, L. D., Martin, A. C., & Emery, J. P. 2025, Measuring the Effects of Regolith Porosity on Mid-IR Spectra of the Allende Meteorite, PSJ, 6, 54
DeMeo, F., & Carry, B. 2013, The Taxonomic Distribution of Asteroids from Multi-filter All-sky Photometric Surveys, Icar, 226, 723
DeMeo, F. E., Binzel, R. P., Carry, B., Polishook, D., & Moskovitz, N. A. 2014, Unexpected D-type Interlopers in the Inner Main Belt, Icar, 229, 392
Donaldson Hanna, K., Bowles, N., Warren, T., et al. 2021, Spectral Characterization of Bennu Analogs Using PASCALE: A New Experimental Set-up for Simulating the Near-surface Conditions of Airless Bodies, JGRE, 126, e2020JE006624
Emery, J., & Brown, R. 2004, The Surface Composition of Trojan Asteroids: Constraints Set by Scattering Theory, Icar, 170, 131
Emery, J., Cruikshank, D., & Van Cleve, J. 2006, Thermal Emission Spectroscopy (5.2–38 μm) of Three Trojan Asteroids with the Spitzer Space Telescope: Detection of Fine-grained Silicates, Icar, 182, 496
Emery, J. P., Burr, D. M., & Cruikshank, D. P. 2010, Near-infrared Spectroscopy of Trojan Asteroids: Evidence for Two Compositional Groups, AJ, 141, 25
Fernández, Y. R., Sheppard, S. S., & Jewitt, D. C. 2003, The Albedo Distribution of Jovian TrojanAsteroids, AJ, 126, 1563
Fujiya, W., Sugiura, N., Sano, Y., & Hiyagon, H. 2013, Mn–Cr Ages of Dolomites in CI Chondrites and the Tagish Lake Ungrouped Carbonaceous Chondrite, E&PSL, 362, 130
Gardner, J. P., Mather, J. C., Clampin, M., et al. 2006, The James Webb Space Telescope, SSRv, 123, 485
Gartrelle, G. M., Hardersen, P. S., Izawa, M. R., & Nowinski, M. C. 2021, Illuminating the Dark Side of the Asteroid Population: Visible Near-infrared (0.7–2.45 μm) Surface Mineralogy Modeling of D-type Asteroids Using Shkuratov Theory, Icar, 354, 114043
Gradie, J., & Veverka, J. 1980, The Composition of the Trojan Asteroids, Natur, 283, 840
Grimm, R. E., & McSween, H. Y. 1989, Water and the Thermal Evolution of Carbonaceous Chondrite Parent Bodies, Icar, 82, 244
Hamilton, V. E. 2010, Thermal Infrared (Vibrational) Spectroscopy of Mg–Fe Olivines: A Review and Applications to Determining the Composition of Planetary Surfaces, ChEG, 70, 7
Harish, Hayne, P., Emery, J., et al. 2025, Surface Composition of Asteroid 269 Justitia: Insights from Spectral Mixture Modeling, ApJ, 992, 125
Hasegawa, S., Marsset, M., DeMeo, F. E., et al. 2021, Discovery of Two TNO-like Bodies in the Asteroid Belt, ApJL, 916, L6
Hopp, T., Dauphas, N., Abe, Y., et al. 2022, Ryugu's Nucleosynthetic Heritage from the Outskirts of the Solar System, SciA, 8, eadd8141
Howard, K., Alexander, C. O., Schrader, D., & Dyl, K. 2015, Classification of Hydrous Meteorites (CR, CM and C2 Ungrouped) by Phyllosilicate Fraction: PSD-XRD Modal Mineralogy and Planetesimal Environments, GeCoA, 149, 206
Howard, K., Benedix, G., Bland, P., & Cressey, G. 2010, Modal Mineralogy of CV 3 Chondrites by X-ray Diffraction (PSD-XRD), GeCoA, 74, 5084
Humes, O. A., Martin, A. C., Thomas, C. A., & Emery, J. P. 2024, Comparative Mid-infrared Spectroscopy of Dark, Primitive Asteroids: Does Shared Taxonomic Class Indicate Shared Silicate Composition?, PSJ, 5, 108
Ikeda, Y. 1992, An Overview of the Research Consortium, "Antarctic Carbonaceouschondrites with CI Affinities, Yamato-86720, Yamato-82162, and Belgica-7904", in Proc. NIPR Symp. on Antarctic Meteorites, 5 (National Institute of Polar Research), 49

Izawa, M., King, P., Vernazza, P., Berger, J. A., & McCutcheon, W. 2021, Salt–A Critical Material to Consider When Exploring the Solar System, Icar, 359, 114328
Jewitt, D. C., & Luu, J. X. 1990, CCD Spectra of 591 Asteroids. II-The Trojans as Spectral Analogs of 592 Cometary Nuclei, AJ, 100, 933
Kelley, M. S., Woodward, C. E., Gehrz, R. D., Reach, W. T., & Harker, D. E. 2017, Mid-infrared Spectra of Comet Nuclei, Icar, 284, 344
King, A. J., Bates, H. C., Krietsch, D., et al. 2019, The Yamato-type (CY) Carbonaceous Chondrite Group: Analogues for the Surface of Asteroid Ryugu?, ChEG, 79, 125531
King, A. J., Schofield, P., Howard, K., & Russell, S. 2015, Modal Mineralogy of CI and CI-like Chondrites by X-ray Diffraction, GeCoA, 165, 148
Koike, C., Chihara, H., Tsuchiyama, A., et al. 2003, Compositional Dependence of Infrared Absorption Spectra of Crystalline Silicate-II. Natural and Synthetic Olivines, A&A, 399, 1101
Lacerda, P., & Jewitt, D. C. 2007, Densities of Solar System Objects from Their Rotational Light Curves, AJ, 133, 1393
Lane, M. D., Glotch, T. D., Dyar, M. D., et al. 2011, Midinfrared Spectroscopy of Synthetic Olivines: Thermal Emission, Specular and Diffuse Reflectance, and Attenuated Total Reflectance Studies of Forsterite to Fayalite, JGRE, 116, E08010
Levison, H. F., Bottke, W. F., Gounelle, M., et al. 2009, Contamination of the Asteroid Belt by Primordial Trans-Neptunian Objects, Natur, 460, 364
Levison, H. F., Shoemaker, E. M., & Shoemaker, C. S. 1997, Dynamical Evolution of Jupiter's Trojan Asteroids, Natur, 385, 42
Levison, H. F., Olkin, C. B., Noll, K. S., et al. 2021, Lucy Mission to the Trojan Asteroids: Science Goals, PSJ, 2, 171
Lowry, V. C., Hanna, K. L. D., Ito, G., et al. 2022, T-matrix and Hapke Modeling of the Thermal Infrared Spectra of Trojan Asteroids and (944) Hidalgo: Implications for Their Regolith Particle Size and Porosity, PSJ, 3, 181
MacLennan, E., & Granvik, M. 2024, Thermal Decomposition as the Activity Driver of Near-Earth Asteroid (3200) Phaethon, NatAs, 8, 60
Marchis, F., Descamps, P., Hestroffer, D., & Berthier, J. 2005, Discovery of the Triple Asteroidal System 87 Sylvia, Natur, 436, 822
Marchis, F., Hestroffer, D., Descamps, P., et al. 2006, A Low Density of 0.8 g cm-3 for the Trojan Binary Asteroid 617 Patroclus, Natur, 439, 565
Martin, A., Emery, J., & Loeffler, M. 2022, Spectral Effects of Regolith Porosity in the Mid-IR–Forsteritic Olivine, Icar, 378, 114921
Martin, A., Emery, J., & Loeffler, M. 2023, Spectral Effects of Regolith Porosity in the Mid-IR–Pyroxene, Icar, 397, 115507
Martin, A. C., & Emery, J. P. 2023, MIR Spectra and Analysis of Jovian Trojan Asteroids, PSJ, 4, 153
Martin, A. C., Emery, J. P., Loeffler, M., & Donaldson Hanna, K. L. 2025, Mid-infrared Reflectance and Emissivity Spectra of High Porosity Regoliths, JGRE, 130, e2024JE008331
Matsuoka, K., Nakamura, T., Nakamuta, Y., & Takaoka, N. 1996, Yamato-86789: A Heated CM-like Carbonaceous Chondrite, in Proc. NIPR Symp. on Antarctic Meteorites, 9 (National Institute of Polar Research), 20
Morbidelli, A., Levison, H. F., Tsiganis, K., & Gomes, R. 2005, Chaotic Capture of Jupiter's Trojan Asteroids in the Early Solar System, Natur, 435, 462
Nakamura, T. 2005, Post-hydration Thermal Metamorphism of Carbonaceous Chondrites, JMPeS, 100, 260
Nakamura, T., Matsumoto, M., Amano, K., et al. 2022, Formation and Evolution of Carbonaceous Asteroid Ryugu: Direct Evidence from Returned Samples, Sci, 379, eabn8671
Neese, C. 2010, Asteroid Taxonomy V6. 0, NASA Planetary Data System,
Nesvorný, D., Vokrouhlický, D., & Morbidelli, A. 2013, Capture of Trojans by Jumping Jupiter, ApJ, 768, 45
Nicodemus, F. E. 1965, Directional Reflectance and Emissivity of an Opaque Surface, ApOpt, 4, 767
O'Rourke, L., Müller, T. G., Biver, N., et al. 2020, Low Water Outgassing from (24) Themis and (65) Cybele: 3.1 μm near-IR Spectral Implications, ApJL, 898, L45
Palguta, J., Schubert, G., & Travis, B. J. 2010, Fluid Flow and Chemical Alteration in Carbonaceous Chondrite Parent Bodies, E&PSL, 296, 235
Perna, D., Bott, N., Hromakina, T., et al. 2018, Rotationally Resolved Spectroscopy of Jupiter Trojans (624) Hektor and (911) Agamemnon, MNRAS, 475, 974
Reddy, V., Sanchez, J. A., Nathues, A., et al. 2012, Photometric, Spectral Phase and Temperature Effects on 4 Vesta and HED Meteorites: Implications for the Dawn Mission, Icar, 217, 153
Rivkin, A., Binzel, R., & Bus, S. 2005, Constraining Near-Earth Object Albedos Using Near-infrared Spectroscopy, Icar, 175, 175
Rubin, A. E. 2012, Collisional Facilitation of Aqueous Alteration of CM and CV Carbonaceous Chondrites, GeCoA, 90, 181
Salisbury, J. 1993, Mid-infrared Spectroscopy: Laboratory Data, Remote Geochemical Analysis: Elemental and Mineralogical Composition (Cambridge Univ. Press), 79
Salisbury, J. W., D'Aria, D. M., & Jarosewich, E. 1991, Midinfrared (2.5–13.5 μm) Reflectance Spectra of Powdered Stony Meteorites, Icar, 92, 280
Schrader, D. L., Torrano, Z. A., Foustoukos, D. I., et al. 2025, Reassessing the Proposed "CY chondrites": Evidence for Multiple Meteorite Types and Parent Bodies from Cr-Ti-HCN Isotopes and Bulk Elemental Compositions, GeCoA, 390, 24
Sharkey, B. N., Rivkin, A. S., Cartwright, R. J., et al. 2025, JWST Reveals Varied Origins between Jupiter's Irregular Satellites arxiv:2501.16484
Stansberry, J., Van Cleve, J., Reach, W., et al. 2004, Spitzer Observations of the Dust Coma and Nucleus of 29P/Schwassmann-Wachmann 1, ApJS, 154, 463
Sultana, R., Poch, O., Beck, P., et al. 2023, Reflection, Emission, and Polarization Properties of Surfaces Made of Hyperfine Grains, and Implications for the Nature of Primitive Small Bodies, Icar, 395, 115492
Suttle, M., King, A., Harrison, C., et al. 2023, The Mineralogy and Alteration History of the Yamato-type (CY) Carbonaceous Chondrites, GeCoA, 361, 245
Suttle, M. D., Daly, L., Jones, R. H., et al. 2024, The Winchcombe Meteorite —A Regolith Breccia from a Rubble Pile CM Chondrite Asteroid, M&PS, 59, 1043
Tedesco, E. F., Noah, P. V., Noah, M., & Price, S. D. 2002, The Supplemental IRAS Minor Planet Survey, AJ, 123, 1056
Vernazza, P., Delbo, M., King, P., et al. 2012, High Surface Porosity as the Origin of Emissivity Features in Asteroid Spectra, Icar, 221, 1162
Vernazza, P., Ferrais, M., Jorda, L., et al. 2021, VLT/SPHERE Imaging Survey of the Largest Main-belt Asteroids: Final Results and Synthesis, A&A, 654, A56
Vernazza, P., Fulvio, D., Brunetto, R., et al. 2013, Paucity of Tagish Lake-like Parent Bodies in the Asteroid Belt and among Jupiter Trojans, Icar, 225, 517
Vernazza, P., Marsset, M., Beck, P., et al. 2015, Interplanetary Dust Particles as Samples of Icy Asteroids, ApJ, 806, 204
Vilas, F., & Gaffey, M. J. 1989, Phyllosilicate Absorption Features in Main-belt and Outer-belt Asteroid Reflectance Spectra, Sci, 246, 790
Wong, I., & Brown, M. E. 2016, A Hypothesis for the Color Bimodality of Jupiter Trojans, AJ, 152, 90
Wong, I., Brown, M. E., Emery, J. P., et al. 2024, JWST Near-infrared Spectroscopy of the Lucy Jupiter Trojan Flyby Targets: Evidence for OH Absorption, Aliphatic Organics, and CO2, PSJ, 5, 87
Yang, B., & Jewitt, D. 2011, A Near-infrared Search for Silicates in Jovian Trojan Asteroids, AJ, 141, 95
Yang, B., Lucey, P., & Glotch, T. 2013, Are Large Trojan Asteroids Salty? An Observational, Theoretical, and Experimental Study, Icar, 223, 359